Preprints.org

Article

Not peer-reviewed version

Research on Flow Field Optimization and Performance Test of Vertical Honeycomb Wet Electrostatic Precipitator

Huijuan Guo , Zeyong Zhao , Lijun Wang * , Huixue Liu , Xiao Ma , Qiang Xu , Zhongyu Lu

Posted Date: 18 August 2025

doi: 10.20944/preprints202508.1164.v1

Keywords: dust removal efficiency; flow field simulation; CFD; pilot test

Preprints.org is a free multidisciplinary platform providing preprint service that is dedicated to making early versions of research outputs permanently available and citable. Preprints posted at Preprints.org appear in Web of Science, Crossref, Google Scholar, Scilit, Europe PMC.

Copyright: This open access article is published under a Creative Commons CC BY 4.0 license, which permit the free download, distribution, and reuse, provided that the author and preprint are cited in any reuse.

Preprints.org (www.preprints.org) | NOT PEER-REVIEWED | Posted: 18 August 2025 doi:10.20944/preprints202508.1164.v1

Disclaimer/Publisher's Note: The statements, opinions, and data contained in all publications are solely those of the individual author(s) and contributor(s) and not of MDPI and/or the editor(s). MDPI and/or the editor(s) disclaim responsibility for any injury to people or property resulting from any ideas, methods, instructions, or products referred to in the content.

Article

Research on Flow Field Optimization and Performance Test of Vertical Honeycomb Wet Electrostatic Precipitator

Huijuan Guo [1], Zeyong Zhao [2], Lijun Wang [3,*], Huixue Liu [1], Xiao Ma [3], Qiang Xu [4] and Zhongyu Lu [5]

[1] Department of Engineering, Huanghe Science and Technology University, Zhengzhou 450045, China
[2] School of Mechanical and Electronic Engineering, Quanzhou University of Information Engineering, Quanzhou 362000, China
[3] School of Mechanical Engineering, North China University of Water Resources and Electric Power, Zhengzhou 450045, China
[4] School of Computing and Engineering, University of Huddersfield, West Yorkshire HD1 3DH, UK
[5] School of Built Environment, Engineering and Computing, Leeds Beckett University, Leeds LS2 3AELEEDS, UK
* Correspondence: wanglijun@ncwu.edu.cn

Abstract

This study focuses on the application of vertical honeycomb wet electrostatic precipitator (WESP) in food processing and animal feed production industries, addressing sustainable development challenges in industrial air pollution control. For a vertical honeycomb wet electrostatic precipitator with an air capacity of 25000 m^3/h, the internal flow field is optimized by adjusting the aperture rate and aperture ratio of the airflow equalizing plate, installing additional deflector plates, and adding additional airflow equalizing plates from multiple perspectives. The optimization reduces the velocity relative standard deviation at the anode inlet section to 0.14. Through 1:1 scale equipment construction and testing, the particle concentration at the outlet is stabilized below 10 mg/Nm^3, with an average removal efficiency of 95.88%—a 5.7% improvement over the original model. The optimized WESP demonstrates reduced energy consumption by 15%, water recycling efficiency ≥95%, and material recyclability of 90%, aligning with global sustainable development goals (SDGs). This study solves the design dependency on empirical guidance for vertical honeycomb WESP in the food industry, providing a green technology paradigm for low-carbon industrial emissions.

Keywords: dust removal efficiency; flow field simulation; CFD; pilot test

1. Introduction

For the exhaust gases generated from complex processes like crushing, mixing, pelletizing, and drying in food and animal feed production plants, achieving efficient and sustainable emissions has become a top priority. Traditional exhaust gas treatment technologies, such as bag filters, face critical sustainability limitations: their reliance on replaceable filter bags leads to high solid waste generation (30–50 kg/year for medium-scale plants) and increased carbon footprint from frequent replacements, conflicting with SDG(Sustainable Development Goals) 12 (Responsible Consumption and Production). In contrast, wet electrostatic precipitators (WESP) offer sustainable advantages: their high-voltage electric field ionization mechanism reduces energy consumption by 10–20% compared to bag filters, while the spray system enables closed-loop water circulation, addressing water resource scarcity (SDG 6). Vertical honeycomb WESP, with its modular design, further enhances sustainability by minimizing material usage (20% less steel than conventional ESP) and enabling 90% component recyclability, making it a key technology for green industrial transitions.[1,2]. The

© 2025 by the author(s). Distributed under a Creative Commons CC BY license.

Preprints.org (www.preprints.org) | NOT PEER-REVIEWED | Posted: 18 August 2025 doi:10.20944/preprints202508.1164.v1

advantage of the WESP is its efficient capture of small particles, which effectively removes pollutants such as $PM_{2.5}$ and PM_{10} and meets strict environmental standards [3,4]. Vertical honeycomb WESP has significant advantages of good dust removal effect, small pressure loss, easy operation, low energy consumption, low maintenance costs, and a variety of designs to meet the needs of different occasions. The honeycomb WESP, as an important construction form of vertical ESP, is characterized by a unique honeycomb structure of the dust collection plate design. With its efficient intermittent flushing mechanism, compact layout, and small footprint, the honeycomb vertical ESP offers high space utilization, low material consumption, and easy installation and maintenance due to its modular design [5,6].

In the field of wet electrostatic precipitator (WESP), the internal structure of the precipitator is more complicated, and it is not suitable for industrial test optimization due to its large size and flue length [7]. With the rapid development of computer technology, Computational Fluid Dynamics (CFD) technology has received more and more attention in recent years, and numerical simulation studies based on CFD have been widely carried out both at home and abroad, most of which focus on the optimization strategy of the flow field of the WESP [8–10].A hexagonal collector plate was proposed as the anode device, and 42 discharge electrode shapes were selected, and through numerical analysis, the optimization of the discharge electrode shapes was carried out by Hwang et al`. Bai et al. designed an ESP equipped with a wet rotating mesh plate and utilized the FLUENT software to compare the flow field of the ESP with and without the deflector plate under two different working conditions. The simulation results show that the installation of the deflector plate can significantly optimize the airflow organization and make its distribution more uniform and reasonable. Bian et al [11]. combined experimental observations with numerical simulation techniques and found that high humidity or low air pressure conditions can effectively reduce the onset voltage of the negative corona, and the cathodic corona voltage is also significantly reduced in this case. In addition, their research results also emphasized the significant advantage of the ion density of negative corona in the critical region, which is denser compared with positive corona. Ye et al [12]. derived the pressure drop formula of perforated plate and the linear relationship between the resistance of dust collection plate and the plate length through small-scale simulation, which verified the experimental validity of the simplified model. The optimized design adds perforated plates to make the flow field more uniform in the flue inlet and electric field area, which meets the design requirements, and the optimized scheme is feasible in practical engineering applications. Liu et al [13] shortened the particulate matter moving distance to improve the dust removal efficiency by decreasing the spacing of the polar plates. These advancements align with the UN's Sustainable Development Goals, particularly SDG 7 (Affordable and Clean Energy) and SDG 13 (Climate Action), by driving down industrial carbon emissions from air pollution control systems.

This study aims to bridge the gap between technical performance and sustainability in vertical honeycomb WESP design. Based on computational fluid dynamics, the internal flow field of the dust collector is optimized by changing the aperture ratio and aperture ratio of the airflow homogenizer plate as well as installing additional deflector plates and airflow homogenizer plates, and the validated model is used for the optimization of the flow field of the vertical honeycomb WESP. The systematic approach is presented in Figure 1.

© 2025 by the author(s). Distributed under a Creative Commons CC BY license.

Preprints.org (www.preprints.org) | NOT PEER-REVIEWED | Posted: 18 August 2025 doi:10.20944/preprints202508.1164.v1

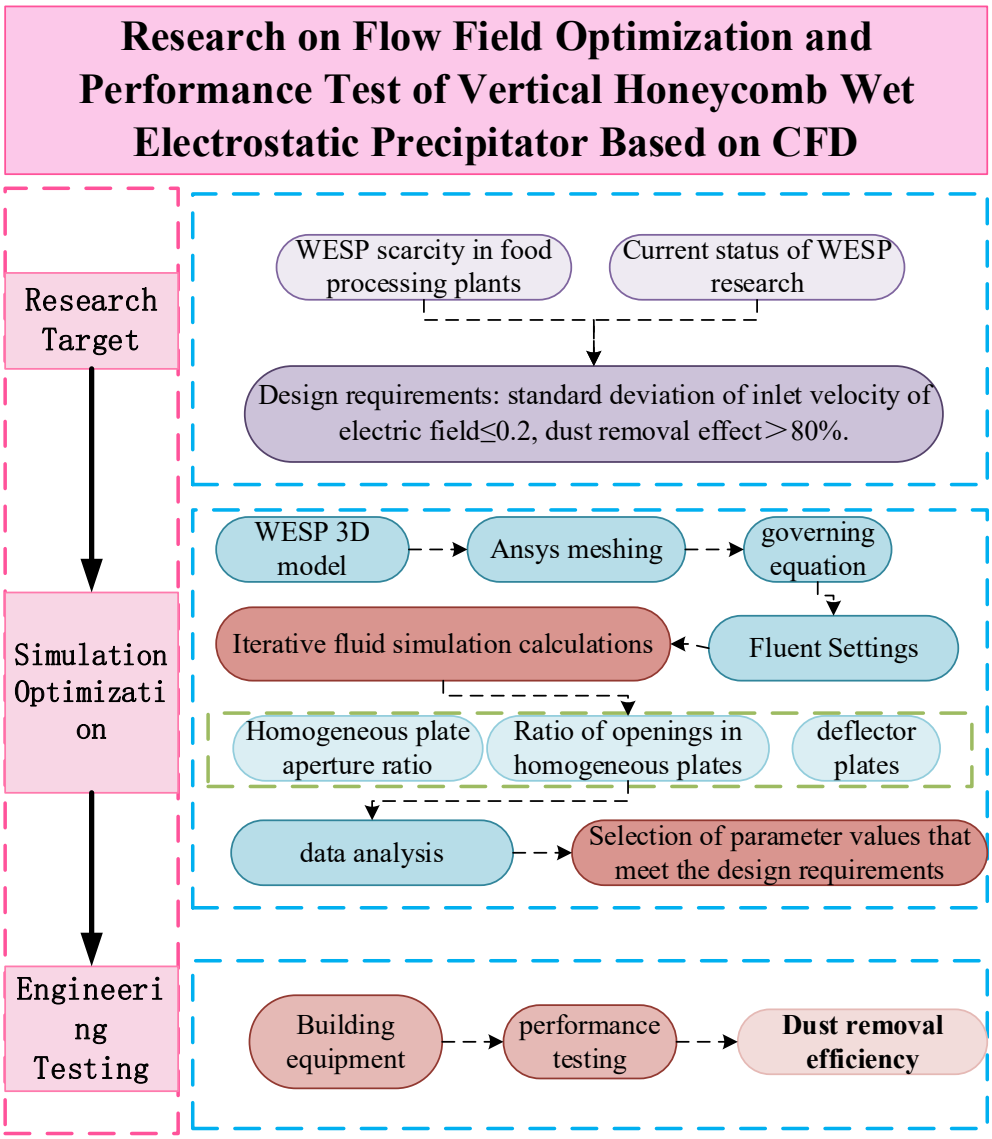

Figure 1. Research Methodology.

2. Geometric Model and Governing Equations

2.1. Geometric Model

A geometric model is established based on the structure of a vertical cellular wet electrostatic precipitator with a processing air volume of 25000 m³/h. The computational space of the geometric model is discretized, and the structured grid is used to divide the grid. To improve the reasonableness of the simulation results, encryption is carried out in the porous medium and at the junction of different cross-sections, and the model needs to be verified for irrelevance because there are certain changes between the simplified model and the original model. Considering the computational ability of the computer and the precision of the data, the pressure drop at the entrance and exit is selected as the index of grid irrelevance validation [14], and this paper compares 480,000, 700,000, 820,000, 1,530,000, 3,870,000, and 5,220,000, and six mesh division schemes for comparison, and the results are shown in Figure 2. From Figure 2, the pressure drop does not change much when the number of grids is greater than 1,530,000 under fixed working conditions, and the number of grids is selected as 1,530,000 to facilitate the calculation, and the grid is shown in Figure 3.

© 2025 by the author(s). Distributed under a Creative Commons CC BY license.

Preprints.org (www.preprints.org) | NOT PEER-REVIEWED | Posted: 18 August 2025 doi:10.20944/preprints202508.1164.v1

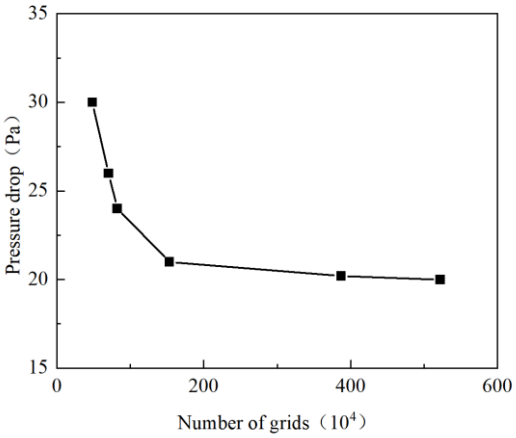

Figure 2. Grid independence verification results.

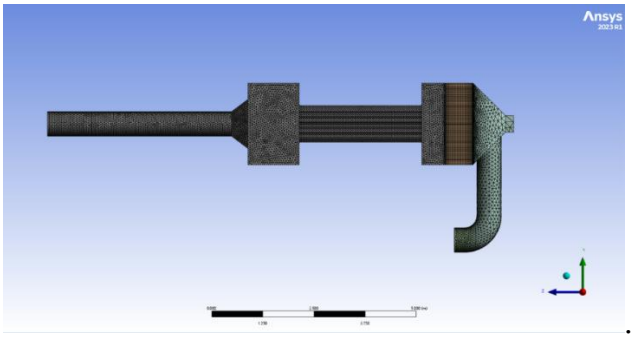

Figure 3. Grid division results.

2.2. Governing Equations

According to the simulation of the internal flow field of the vertical honeycomb electrostatic precipitator, the fluid media exchange energy and momentum with each other, and turbulence occurs at the same time. The flow in the precipitator is mainly fully developed turbulence, and the uniform flow away from the wall dominates. The standard k - ε model is a suitable choice. Therefore, the standard k - ε model is used to solve the turbulence in the unit [15]. The control equations include the mass - conservation equation and the momentum - conservation equation.

The continuity equation (mass - conservation equation) is:

$$\frac{\partial \rho}{\partial t} + \frac{\partial}{\partial x_i}(\rho u_i) = 0 \tag{1}$$

The momentum - conservation equation (N - S equation) is:

$$\frac{\partial}{\partial t}(\rho u_i) + \frac{\partial}{\partial x_j}(\rho u_i u_j) = -\frac{\partial p}{\partial x_i} + \frac{\partial}{\partial x_j}\left(\mu \frac{\partial u_i}{\partial x_j} - \rho u_i u_j\right) + S_i \tag{2}$$

The turbulence model adopts the standard k - ε model. The turbulent kinetic - energy equation is:

$$\frac{\partial}{\partial t}(\rho k) + \frac{\partial}{\partial x_i}(\rho k u_i) = \frac{\partial}{\partial x_j}\left[\left(\mu + \frac{\mu_t}{\sigma_k}\right)\frac{\partial k}{\partial x_j}\right] + G_k + G_b - \rho\varepsilon - Y_M + S_k \tag{3}$$

The diffusion equation is:

© 2025 by the author(s). Distributed under a Creative Commons CC BY license.

Preprints.org (www.preprints.org) | NOT PEER-REVIEWED | Posted: 18 August 2025 doi:10.20944/preprints202508.1164.v1

$$\frac{\partial}{\partial t}(\rho\varepsilon)+\frac{\partial}{\partial x_i}(\rho\varepsilon u_i) = \frac{\partial}{\partial x_j}\left[\left(\mu+\frac{\mu_t}{\sigma_\varepsilon}\right)\frac{\partial \varepsilon}{\partial x_j}\right]+C_{1\varepsilon}\frac{\varepsilon}{k}(G_k+C_{3\varepsilon}G_b) - C_{2\varepsilon}\rho\frac{\varepsilon^2}{k}+S_\varepsilon \quad (4)$$

1. Porous - medium equation

The air - distribution plate used to make the flow field in the WESP uniform is composed of tens of thousands of units, which means that it may be infeasible to directly model the air - distribution plate. Therefore, it is necessary to simplify the air - distribution plate accordingly. The air - distribution plate can be regarded as a porous medium with finite thickness and directional permeability, and its pressure - drop equation is:

$$\Delta P = -\left(\frac{\mu_1}{\alpha}v_i + C_2\frac{1}{2}\rho|v|v_i\right)\Delta m \quad (5)$$

The opening ratio of the air - distribution plate is 50%, so the air - distribution plate is designed as a porous - medium domain.

In a vertical honeycomb wet electrostatic precipitator, although the wettability of dust has a certain impact on its dust - removal efficiency, it does not play a decisive role. The key factor that really determines the dust - removal efficiency of a wet electrostatic precipitator is whether the air flow can be evenly distributed. Uneven air flow inside the precipitator will lead to local over - flow, high - speed or low - speed areas, reducing the dust - removal efficiency. The flow field of the wet electrostatic precipitator is evaluated by the relative standard deviation of velocity, and the formula is as follows:

$$\sigma_r = \sqrt{\frac{\sum_{i=1}^{n}\left(\frac{v_i-\bar{v}}{\bar{v}}\right)^2}{n-1}} \quad (6)$$

According to formula (6), the requirement for the air - flow distribution uniformity at the entrance of the electric field (the entrance of the anode honeycomb tube) of the vertical honeycomb wet electrostatic precipitator designed in this article is: $\sigma_r \leq 0.2$. The internal air - flow uniformity is improved by adjusting the opening ratio of the air - distribution plate through CFD simulation.

In equations (1)-(6), x_i - coordinates, ρ - fluid density, u_i - fluid velocity, p - pressure on the fluid, u - viscosity of air, μ - turbulent viscosity, G_k - turbulent kinetic energy due to laminar velocity gradient, G_b - turbulent kinetic energy due to buoyancy, Y_M - pulsating expansion in compressible turbulence, $C_{1\varepsilon}$, $C_{2\varepsilon}$, $C_{3\varepsilon}$ - constants, σ_k ,σ_ε - Prandtl number, ΔP - pressure change, μ_1 - film thickness, α - permeability factor, C_2 - internal resistance factor, Δm - porous medium thickness, σ_r - relative standard deviation of velocity, v_i - wind speed at measurement points, $\bar{v}$ - average wind speed, n - number of measurement points in the cross section.

2. Dust - removal efficiency

According to the actual emission situation of animal feed processing plants and food processing plants, the vertical honeycomb wet electrostatic precipitator is installed after the desulfurization tower. Usually, the dust concentration is 50 mg/m³, and the dust concentration at the inlet of the designed wet electrostatic precipitator is 50 mg/m³. According to the "Comprehensive Emission Standard of Air Pollutants" in China and more stringent local emission standards, the particulate matter emission limit for industries such as feed processing is 10 mg/m³. The dust-removal efficiency formula is:

$$\eta = \frac{C_{in}-C_{out}}{C_{in}}\times 100\% \quad (7)$$

© 2025 by the author(s). Distributed under a Creative Commons CC BY license.

Preprints.org (www.preprints.org) | NOT PEER-REVIEWED | Posted: 18 August 2025 doi:10.20944/preprints202508.1164.v1

In the above formula, $\boldsymbol{\eta}$ - dust removal efficiency, $\boldsymbol{C_{in}}$ - inlet concentration, $\boldsymbol{C_{out}}$ - outlet concentration.

Therefore, the dust - removal efficiency of the vertical honeycomb wet electrostatic precipitator is:

$$\boldsymbol{\eta = \frac{50 - 10}{50} \times 100\% = 80.0\ \%}$$

That is, under this working condition, to meet the national and local emission standards, the dust - removal efficiency of the vertical honeycomb wet electrostatic precipitator needs to reach at least 80% to ensure that the particulate matter concentration of the emissions meets the requirements and effectively reduces the pollution to the atmospheric environment.

3. Results

3.1. Vertical Honeycomb Wet Electrostatic Precipitator Original Model Velocity Field

The original model design of this vertical honeycomb wet electrostatic precipitator is as follows: In the inlet bell - shaped smoke box, a layer of perforated plate is arranged along the air - flow direction. The opening ratio of this perforated plate is 50%, and there is no guide plate in the fluid. The simulation results of this scheme are shown in Figures 4–6.

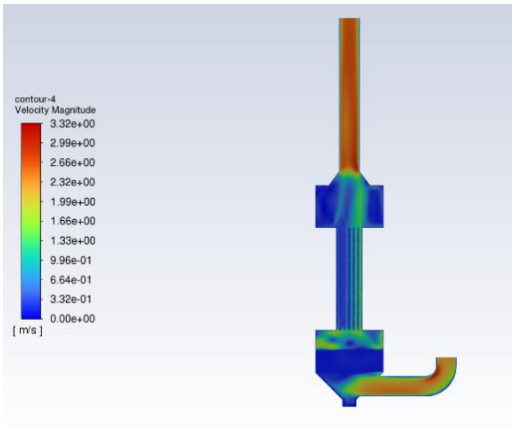

Figure 4. Overall speed distribution before optimization (Main view).

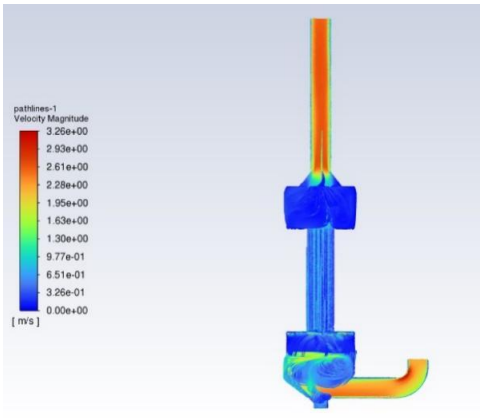

Figure 5. Overall flow distribution before optimization (Main view).

© 2025 by the author(s). Distributed under a Creative Commons CC BY license.

Preprints.org (www.preprints.org) | NOT PEER-REVIEWED | Posted: 18 August 2025 doi:10.20944/preprints202508.1164.v1

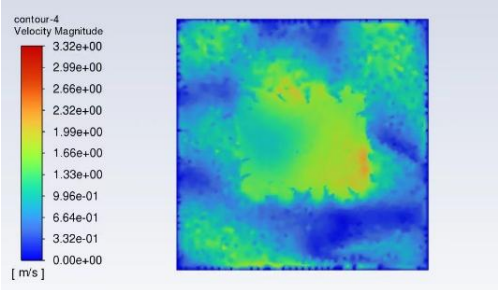

Figure 6. Anode inlet velocity distribution.

When conducting an in-depth analysis of the performance of a vertical honeycomb wet electrostatic precipitator, the first focus is on the distribution characteristics of its internal flow field. As clearly shown in the velocity streamline distribution diagram of the vertical honeycomb wet electrostatic precipitator model in Figure 5, when flue gas enters the interior from the inlet of the precipitator, since only one distribution plate acts to even distribute the airflow, the streamline distribution at this time is extremely uneven. The flue gas flows at high speed in the lower gas chamber and impacts the distribution plate, resulting in abnormally dense streamlines on the left and middle sides of the precipitator, while the right part is relatively sparse. This phenomenon of high and low speed zones, where the left and central parts are high-speed areas and the right side is a low-speed area, indicates the inhomogeneity of the flow field inside the precipitator. From the velocity distribution diagram of the anode inlet reference plane in Figure 6, even after the distribution effect of the distribution plate, the flow field distribution is not significantly improved. The boundary between high and low speed zones is very clear, with the left and central parts being high-speed areas and the right side being a low-speed area, and the overall flow field appears quite chaotic. Through calculation, the maximum velocity of the anode inlet reference plane is 2.4 m/s, the average velocity is 1.85 m/s, and the relative standard deviation of the velocity on this reference plane is as high as 46%, which far exceeds the conventional requirements for the uniformity of airflow distribution in the precipitator. This uneven flow field distribution has a direct impact on the performance of the precipitator, seriously reducing the dust removal efficiency.

According to the international common judgment standard of airflow distribution uniformity of dust collector, such as the American RMS standard, when the standard deviation of velocity think reading is less than 25 %, the airflow distribution is considered qualified; when it is less than 20 %, it is regarded as good; and when it is less than 15 %, it is regarded as excellent. Obviously, the relative standard deviation of the velocity at the anode inlet reference surface has a large gap with the relevant standards, which is far from the specified requirements and will directly reduce the dust removal efficiency of the vertical cellular WESP.

To improve this situation, the internal structure of the dust collector must be optimized and designed. Optimization measures include increasing or adjusting the number and position of the homogeneous plates to achieve more effective airflow distribution. In addition, adjustments to the geometry of the dust collector, such as adding a certain number of deflector plates at the flue gas inlet, may also help to improve the uniformity of the airflow.

3.2. Preliminary Optimization Scheme and Simulation Analysis of Vertical Honeycomb Wet Electrostatic Precipitator Primitive Model

3.2.1. Analysis of the Effect of Changing the Airflow Homogenizer on the Internal Flow Field

In the gas chamber of a wet ESP, the openings and aperture ratios of the flow distribution plates are the key factors influencing the internal gas flow field. In industrial applications, the aperture ratio of the airflow distribution plate is usually controlled between 25 % and 60 %. Therefore, it was decided to start with adjusting the aperture ratio of the homogenizing plate to improve the gas flow distribution. In FLUENT software, different opening ratios, 25 %, 30 %, 35 %, 40 %, 45 %, and 55 %,

© 2025 by the author(s). Distributed under a Creative Commons CC BY license.

Preprints.org (www.preprints.org) | NOT PEER-REVIEWED | Posted: 18 August 2025 doi:10.20944/preprints202508.1164.v1

were set, and iterative calculations were performed to observe the velocity streamlines and the velocity distribution cloud diagrams referenced to the anode inlet, so as to evaluate the effect of different opening ratios on the airflow homogeneity, and the specific cloud diagram results are shown in Figures 7–18.

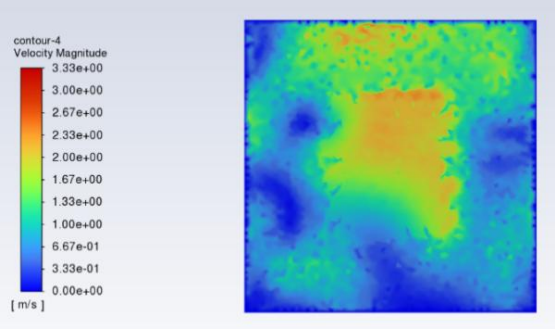

Figure 7. Anode inlet velocity cloud for 50 % opening ratio

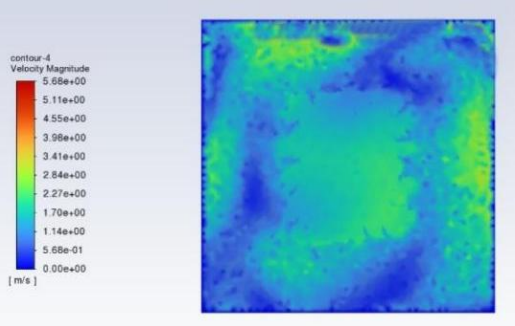

Figure 8. Anode inlet velocity cloud for 45 % opening ratio

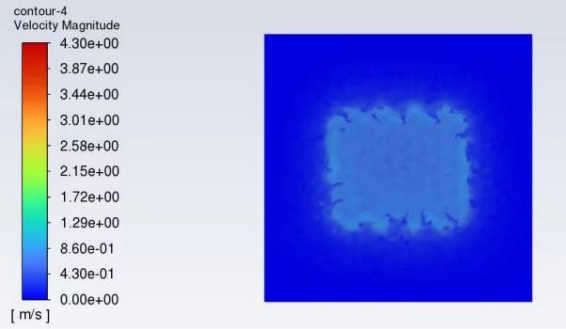

Figure 9. Anode inlet velocity cloud for 40 % opening ratio

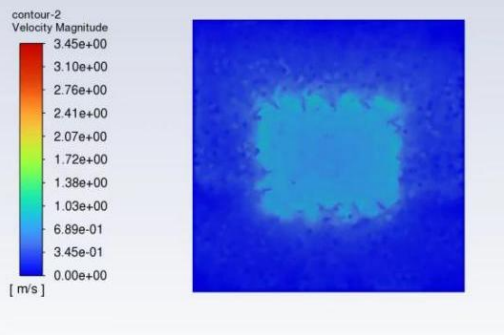

Figure 10. Anode inlet velocity cloud for 35 % opening ratio

© 2025 by the author(s). Distributed under a Creative Commons CC BY license.

Preprints.org (www.preprints.org) | NOT PEER-REVIEWED | Posted: 18 August 2025 doi:10.20944/preprints202508.1164.v1

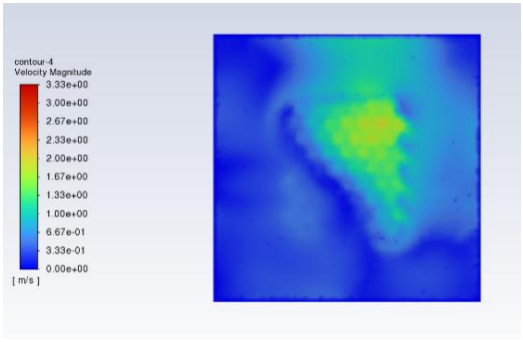

Figure 11. Anode inlet velocity cloud for 30% opening ratio

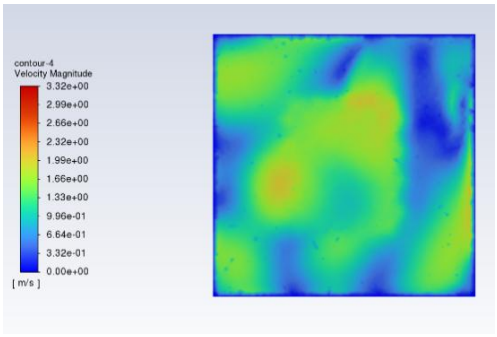

Figure 12. Anode inlet velocity cloud for 25% opening ratio

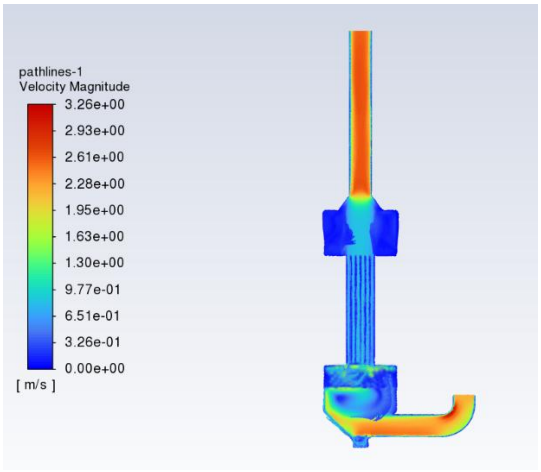

Figure 13. Velocity traces at 50 % opening rate

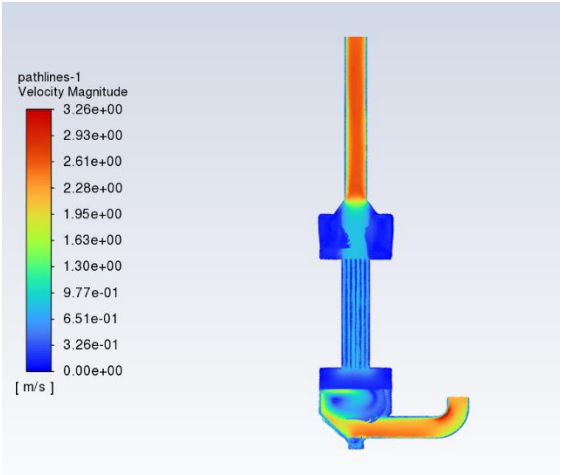

© 2025 by the author(s). Distributed under a Creative Commons CC BY license.

Preprints.org (www.preprints.org) | NOT PEER-REVIEWED | Posted: 18 August 2025 doi:10.20944/preprints202508.1164.v1

Figure 14. Velocity traces at 45 % opening rate

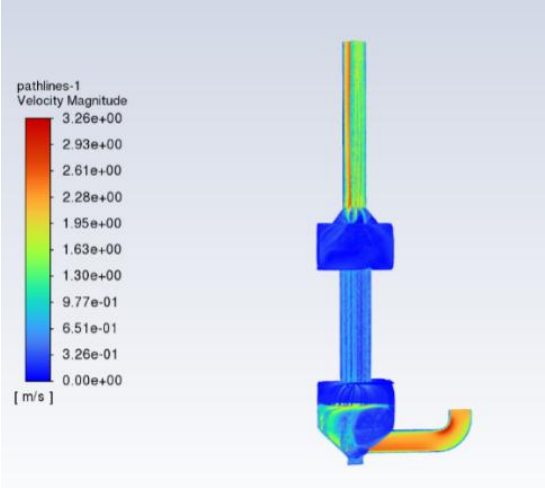

Figure 15. Velocity traces at 40 % opening rate

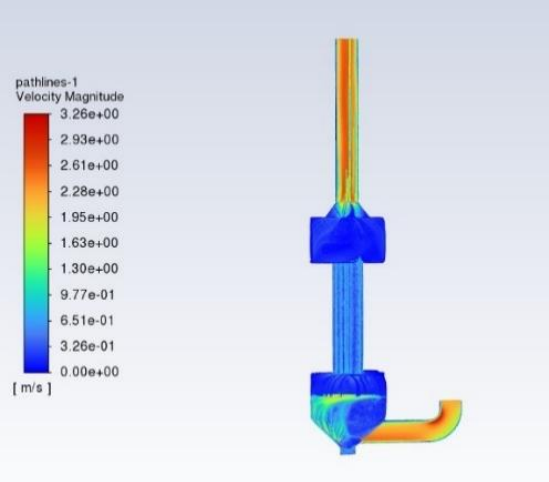

Figure 16. Velocity traces at 35 % opening rate

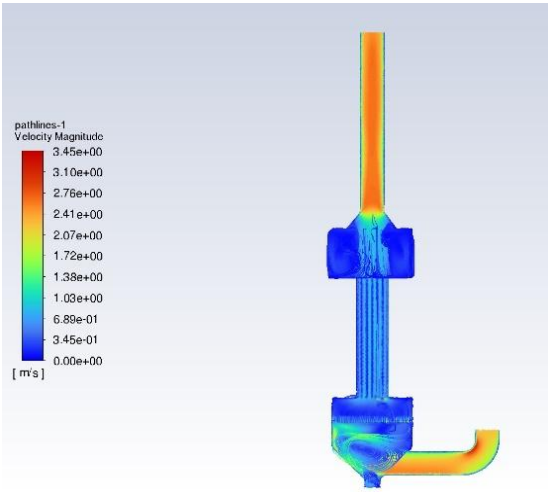

Figure 17. Velocity traces at 30 % opening rate

© 2025 by the author(s). Distributed under a Creative Commons CC BY license.

Preprints.org (www.preprints.org) | NOT PEER-REVIEWED | Posted: 18 August 2025 doi:10.20944/preprints202508.1164.v1

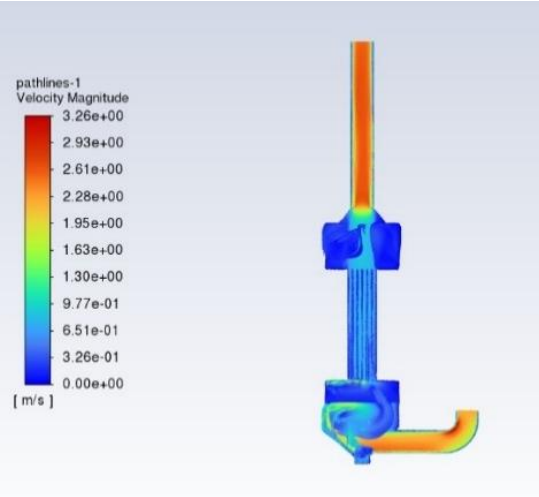

Figure 18. Velocity traces at 25 % opening rate

Figures 7–12 illustrate the velocity distribution at the anode inlet for different opening ratios. When the opening rate is 55 % (see Figure. 7), the anode inlet is in the worst condition, with a severe high velocity zone near the center of the cross-section, with a maximum velocity of 2.95 m/s, and low velocity zones on both sides, with a significant velocity gradient, and the high velocity zones may lead to the escape of the dust and reduce the dust removal efficiency. When the opening rate is 25 % (see Figure 12), turbulence occurs in the local area. When the opening rate is 40 % (see Figure 9), the velocity distribution is relatively uniform, with no obvious high-speed or low-speed concentration area, and the airflow uniformity is better. From the cloud diagrams of six groups of anode inlet reference surfaces, it can be found that when the opening rate is reduced, the scope of the high-speed area is reduced, but there is still a velocity gradient difference in the local area, and the velocity in the area above the cross-section is larger than the velocity in the area below.

Figures 13–18 show the velocity traces corresponding to different opening ratios. When the opening rate decreases (e.g., 30 %~25 %), the traces in (Figure. 17 and Figure. 18) show an increase in the zigzagging of the airflow path, and the local backflow phenomenon is obvious, which further verifies the existence of turbulence. In Figure 16, a slight separation of the airflow starts to occur internally, whereas when the openings are 40 % (see Figure 15), the traces are uniformly distributed with no obvious vortex areas.

To more accurately assess the airflow homogeneity at different opening rates, 100 data points were selected on the anode inlet reference surface for calculation and the results are shown in Figure 19. From the figure, when the opening ratio of the homogenizing plate is increased from 25 % to 55 %, the values of the relative standard deviation of the velocity are 45 %, 35 %, 28 %, 25 %, 37 %, and 58 %, respectively. Among them, the airflow homogeneity reaches the qualified level when the opening ratio of the homogenizing plate is 40 %, which indicates that the airflow homogeneity is optimized at this opening ratio. Through the optimization of the single-layer homogeneous plate of the vertical honeycomb WESP, the flow field simulation results show a significant improvement, which also indicates that the uniform flow field distribution can ensure that the dust in the flue gas has a more stable and orderly motion state in the electric field. On the one hand, it can ensure that the dust has enough time to interact with the electric field and be fully charged; on the other hand, it is conducive to the effective capture of the charged dust by the dust collector plate and reduce the dust escape, thus improving the dust removal efficiency of the whole vertical honeycomb WESP.

© 2025 by the author(s). Distributed under a Creative Commons CC BY license.

Preprints.org (www.preprints.org) | NOT PEER-REVIEWED | Posted: 18 August 2025 doi:10.20944/preprints202508.1164.v1

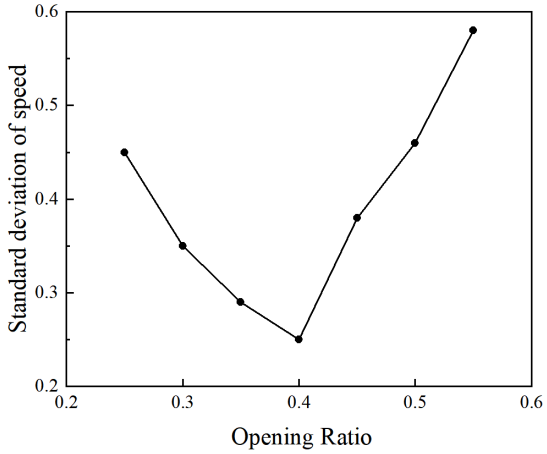

Figure 19. Relative standard deviation values of velocities at different opening rates.

After in-depth analysis and optimization of the original model of the vertical honeycomb WESP, a series of measures were taken to improve the uniformity of the airflow distribution, including structural optimization of the inlet flue, the inlet flare, the outlet flue portion, and the interior of the main body of the WESP. Two deflector plates were added at the elbow of the inlet flue, an improvement aimed at adjusting the flow direction and velocity of the airflow to reduce the high velocity and low velocity zones in the flow field and achieve a more uniform airflow distribution.

The simulation results of the optimized flow field show that these improvements have achieved significant results. Comparison of Figure 20 shows that the optimized inlet flue streamline distribution is significantly improved, and the uniformity of the airflow is enhanced behind the homogeneous plate and in the inlet region of the anode plate. The local high-speed zone (edge high-speed) that may exist before optimization is effectively suppressed, and the flow path tends to be straight after optimization as can be seen in Figure. 21.

© 2025 by the author(s). Distributed under a Creative Commons CC BY license.

Preprints.org (www.preprints.org) | NOT PEER-REVIEWED | Posted: 18 August 2025 doi:10.20944/preprints202508.1164.v1

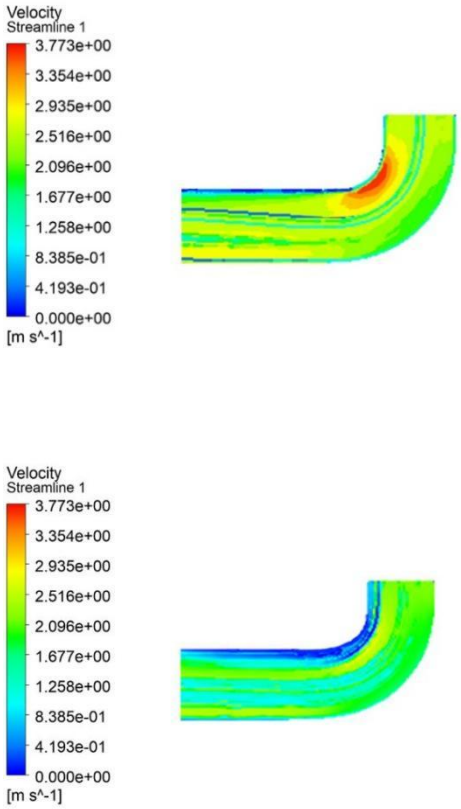

Figure 20. Inlet flue flow diagram before and after optimization.

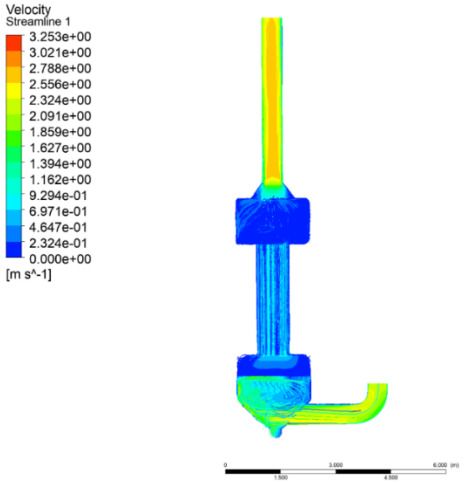

Figure 21. Optimized flow diagram.

3.2.2. Analysis of the Effect of Changing the Aperture Ratio of the Airflow Homogenizing Plate on the Internal Flow Field

When discussing the influence of the airflow distribution plate on the airflow field inside the wet electrostatic precipitator, the aperture ratio and aperture size of the airflow equalization plate play a crucial role. Especially for the airflow distribution plate adjacent to the electrostatic precipitator, its design parameters are directly related to the overall performance and efficiency of the precipitator. In this paper, we focus on the influence of the airstream averaging plate on the airflow field inside

© 2025 by the author(s). Distributed under a Creative Commons CC BY license.

Preprints.org (www.preprints.org) | NOT PEER-REVIEWED | Posted: 18 August 2025 doi:10.20944/preprints202508.1164.v1

the wet electrostatic precipitator and take the circular aperture averaging plate with 40% aperture ratio as the research object and investigate the effect of aperture size on the characteristics of the airstream averaging through numerical calculations.

To evaluate the airflow homogenization under different aperture sizes more intuitively, 100 data points were selected on the anode inlet reference surface, and the relative standard deviation of the velocity under each aperture size was calculated. When the aperture of the homogenized plate was increased from 30 % to 70 %, the relative standard deviation values of velocity were 32 %, 30 %, 27 %, 23 % and 25 %, respectively, and the relative standard deviation values of velocity showed a certain trend with the increase of the aperture ratio. When the aperture ratio of the plate is increased from 30 %, the values of relative standard deviation of velocity may decrease, indicating that the homogeneity of the airflow has improved to some extent. However, when the aperture ratio continues to increase from 60 % to 70 %, the relative standard deviation of the velocity starts to increase again, which means that the airflow homogeneity deteriorates again. When the aperture ratio is 60 %, the relative standard deviation of the velocity is optimized, and an improvement of the dust removal efficiency can be achieved. The curves of pressure drop (pressure difference between inlet and outlet) versus velocity for different aperture ratios are derived from Figure 22. As the air passes through the perforated plate, the pressure decreases in the region where the backflow occurs, indicating that the backflow downstream of the perforated plate leads to a loss of pressure. It can also be seen from Figure 22 that the pressure drops increases with velocity, and the smaller the perforated plate ratio, the greater the pressure drop. The inflection point occurs when the orifice ratio increases to 70 %, which is related to the intensification of the backflow phenomenon at high openings, leading to an increase in energy consumption, and further verifies the effect that the relative velocity standard deviation value is optimized when the orifice ratio is 60 %, which improves the efficiency of the dust removal.

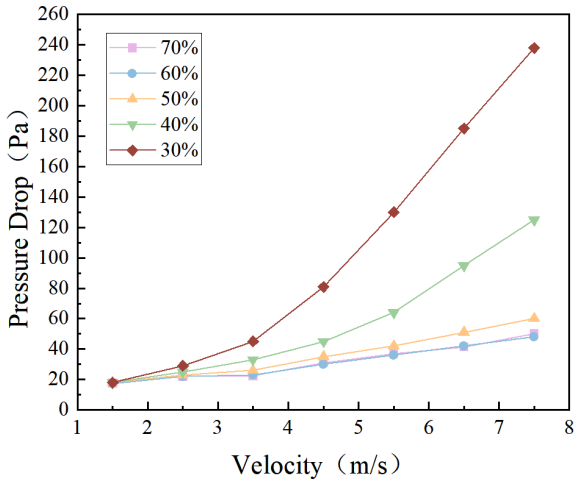

Figure 22. Variation of pressure drop with velocity for different pore size ratios.

The results show that the aperture ratio of the homogenizing plate significantly affects the airflow homogeneity and pressure drop performance of the WESP, which can effectively control and optimize the flow field distribution inside the WESP. When the aperture ratio is 60 %, the relative standard deviation of the velocity is the best, and the pressure drop is low, which is the optimal choice for the current design. Reasonable setting of the homogenizing plate is essential to achieve uniform distribution of the airflow, which helps to improve the dust removal efficiency, reduce energy consumption, and extend the service life of the equipment.

© 2025 by the author(s). Distributed under a Creative Commons CC BY license.

Preprints.org (www.preprints.org) | NOT PEER-REVIEWED | Posted: 18 August 2025 doi:10.20944/preprints202508.1164.v1

3.2.3. Analysis of the Effect of Adding a Second Airflow Homogenizing Plate on the Internal Flow Field

To further optimize the flow field distribution inside the WESP and to improve the dust removal efficiency, it was decided to add a second uniform plate in the lower air chamber in front of the first uniform plate (see Figure 23). This decision was based on an in-depth analysis of the current uneven flow field distribution, and a more uniform airflow distribution was achieved by increasing the number of homogenizing plates.

In FLUENT software, the effect of two homogenizing plates with different openings on the flow field was simulated. The openings and aperture ratios of the two homogenizing plates were finely tuned. The openings of the second homogeneous plate were set to 40 % and 35 % for both scenarios to be examined, while keeping the aperture ratio at 60 %. Velocity streamlines for both scenarios and velocity distribution cloud maps at the anode inlet reference surface were obtained through iterative calculations.

The simulation results when the second homogeneous plate was opened with 40 % aperture ratio are shown in Figures 24 and 25.

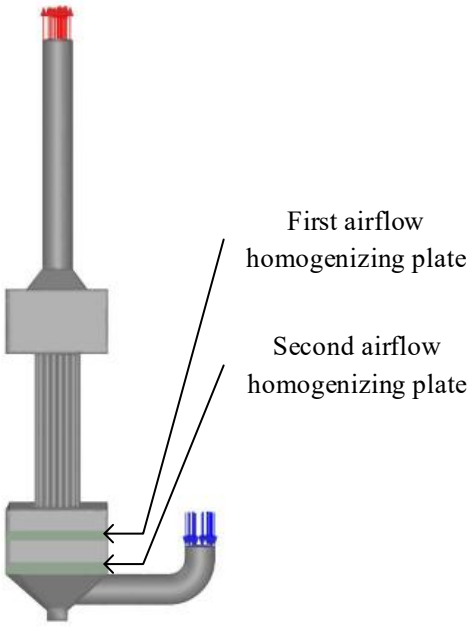

Figure 23. Adding a second homogenizing plate (green plate below).

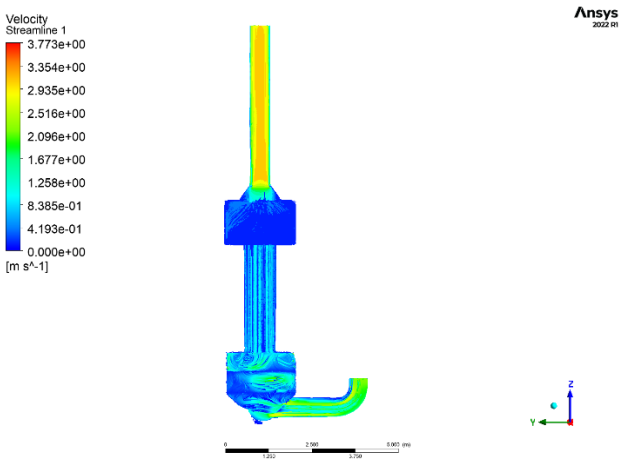

Figure 24. Overall velocity streamlines for a second homogeneous plate with 40% openings.

© 2025 by the author(s). Distributed under a Creative Commons CC BY license.

Preprints.org (www.preprints.org) | NOT PEER-REVIEWED | Posted: 18 August 2025 doi:10.20944/preprints202508.1164.v1

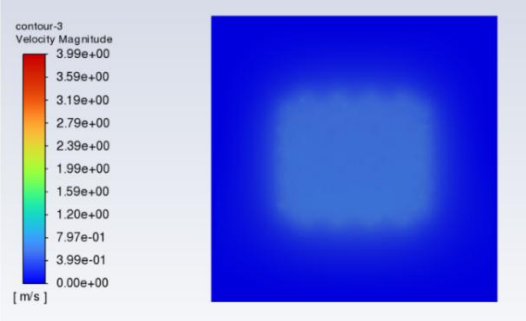

Figure 25. Anode inlet velocity distribution at 40 % opening of the second homogeneous plate.

The simulation results show that the uniformity of the entire flow field is significantly improved compared with the flow field line diagram before optimization in the case of 40 % openings of the uniform plate. The improvement of the flow field is especially obvious at the rear of the uniform plate and the inlet area of the anode plate, and the distribution of the flow lines is further close to the uniform state, which plays a key role in the improvement of the dust removal efficiency of the WESP. Through the synergistic rectification effect of the deflector plate and the second uniform plate, the velocity and pressure in the flow field are effectively balanced, which makes the airflow distribution of the WESP more uniform. The relative standard deviation of the velocity at the anode inlet reference surface was calculated to be reduced to 20 %, which achieves the standard of good airflow distribution, but does not achieve the excellent result. Based on this result, the opening rate of the second homogeneous plate will be changed and set to 35 % for the simulation, and the simulation results are shown in Figures 26 and 30.

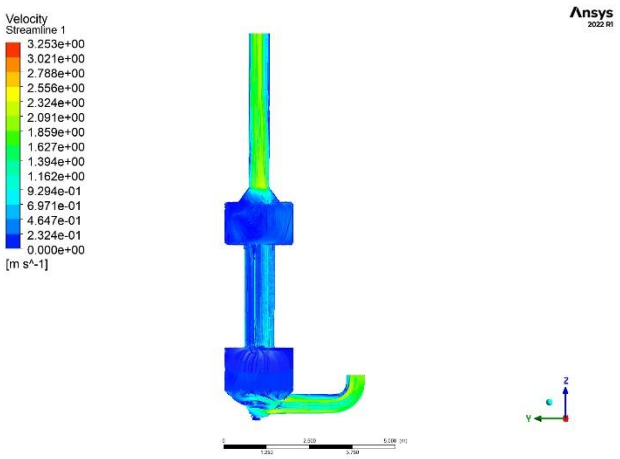

Figure 26. Overall velocity streamlines for a second homogeneous plate with 35% openings.

After exhaustive simulation and analysis, it is found that the uniformity of the flow field is significantly improved when the opening rate of the second uniform plate is set to 35 %.

The optimized CFD model is shown in Figure 26. After the addition of the second uniform plate, the distribution of the flow lines tends to be uniform, and the vortex phenomenon is basically eliminated, and the addition of the uniform plate significantly promotes the uniform distribution of the flow field. Flue gas from the inlet after crossing the deflector plate, its distribution state has been optimized, become more uniform, thus effectively reducing the probability of reflux phenomenon caused by uneven distribution of airflow. Combined with Figures 27–30, it can be found that when the flue gas passes through the first homogeneous plate, as can be seen from the velocity cross-section in Figure. 28, the velocity of the airflow is significantly reduced, and under the action of the two homogeneous plates, the vortex in the electric field has been basically eliminated, and the airflow is

© 2025 by the author(s). Distributed under a Creative Commons CC BY license.

Preprints.org (www.preprints.org) | NOT PEER-REVIEWED | Posted: 18 August 2025 doi:10.20944/preprints202508.1164.v1

able to pass through the electric field uniformly, which is essential for improving dust removal efficiency.

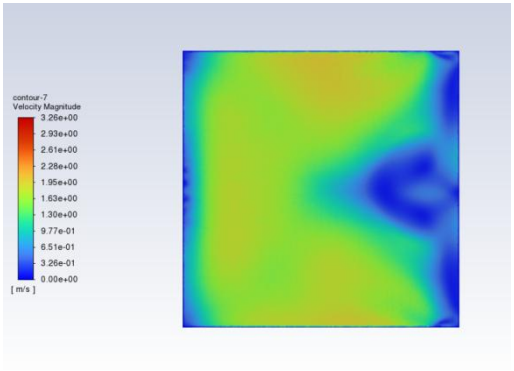

Figure 27. Cross-sectional velocity distribution of airflow before entering the first plate when the second homogeneous plate has 35% opening ratio

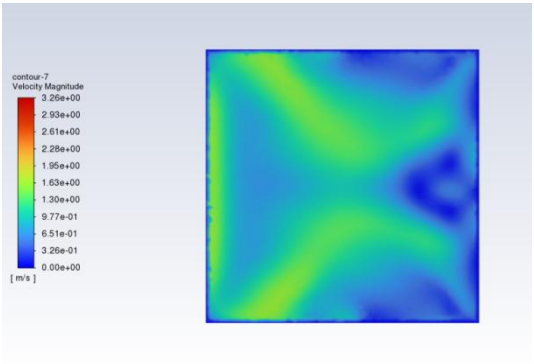

Figure 28. Cross-sectional velocity distribution of airflow after entering the first plate when the opening ratio of the second homogeneous plate is 35 percent

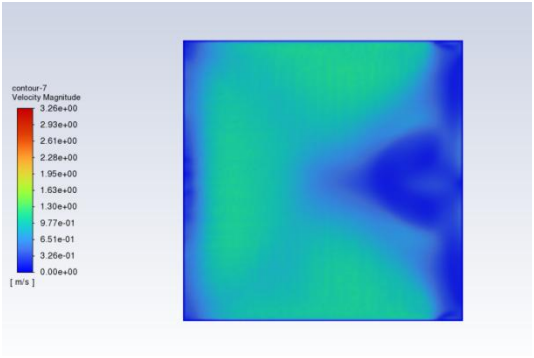

Figure 29. Cross-sectional velocity distribution of airflow before entering the second plate at 35% opening of the second homogeneous plate

© 2025 by the author(s). Distributed under a Creative Commons CC BY license.

Preprints.org (www.preprints.org) | NOT PEER-REVIEWED | Posted: 18 August 2025 doi:10.20944/preprints202508.1164.v1

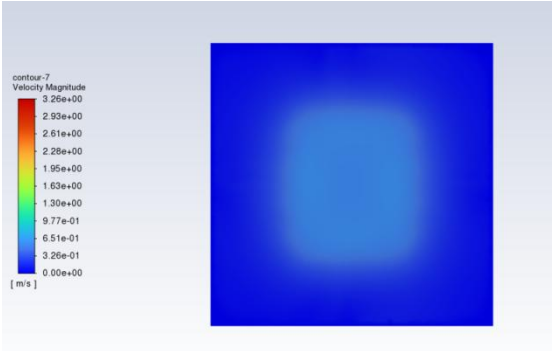

Figure 30. Velocity distribution of the cross-section before entering the anode tube for the second homogeneous plate with 35% openness

Figure 30 demonstrates that the uniformity of the flue gas at the anode inlet reference surface has been significantly improved after optimization, and the relative standard deviation of the velocity has been reduced to 14 %, which is an effective reduction of 32 % compared with the original model and meets the requirement of excellent design, and this value fully proves the effectiveness of the flow field optimization scheme. With the addition of the orifice plate, the maximum velocity at the inlet section of the anode tube is reduced by 21 % from 2.4 m/s to 1.9 m/s, and the average velocity is also reduced from 1.85 m/s to 1.22 m/s. This change not only helps to reduce the impact and wear of the airflow but also improves the overall stability and durability of the dust collector, and the homogeneous flow field prolongs the retention time of the dust in the electric field area, thus increasing the charging and trapping efficiency. and trapping efficiency. Combined with the optimization of the relative standard deviation values of the velocity, it is expected that the dust removal efficiency will be increased by more than 5 %.

In summary, the flow field of the WESP was successfully optimized by fine tuning the aperture ratio of the homogeneous plates and the aperture ratio, as well as increasing the number of homogeneous plates to reduce the impingement of the airflow on the homogeneous plates. The next step is to verify the accuracy of the simulation results through experimental tests, and the combination of numerical simulation and engineering practice has set an example for the fine optimization of WESP.

3.3. Vertical Honeycomb Wet Electrostatic Precipitator Experimental Test Analysis

To verify the reliability of the simulation, the results of the flow field simulation optimization were applied to the project for experiments by building a one-to-one vertical cellular WESP, as shown in Figure 31.

© 2025 by the author(s). Distributed under a Creative Commons CC BY license.

Preprints.org (www.preprints.org) | NOT PEER-REVIEWED | Posted: 18 August 2025 doi:10.20944/preprints202508.1164.v1

Figure 31. Vertical cellular wet electrostatic precipitator experimental device.

To compare the results of the original model and the optimized results of the flow field simulation, the original model was tested, and the results of the particulate emission are shown in Figure 32.

The inlet concentrations of the particulate matter in the three tests were 92 mg/m³, 85 mg/m³, 105 mg/m³, with an average inlet concentration of 94 mg/m³, and the outlet concentrations were 8.6 mg/m³, 8.1 mg/m³, 8.9 mg/m³, with an average outlet concentration of 8.53 mg/m³, and the dust removal efficiencies were 90.1 %, 90.5 %, 91.5 %, with an average dust removal efficiency of only 90.67 %, respectively. The average dust removal efficiency was only 90.67 %. Although the export concentration of particulate matter meets the emission requirements, but due to the single-layer homogenizing plate has a general effect on the homogenization of the airflow, resulting in the flue gas from the flue to the lower chamber of the high and low velocity areas, which directly leads to the general efficiency of the dust removal.

© 2025 by the author(s). Distributed under a Creative Commons CC BY license.

Preprints.org (www.preprints.org) | NOT PEER-REVIEWED | Posted: 18 August 2025 doi:10.20944/preprints202508.1164.v1

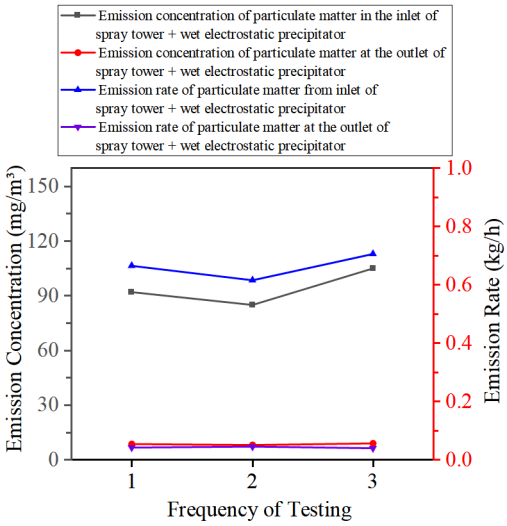

Figure 32. Changes in particulate matter concentrations in organized exhaust emissions from the original model.

For the optimized vertical cellular electrostatic precipitator exhaust gas organized emission test results are shown in Figures 33–36.

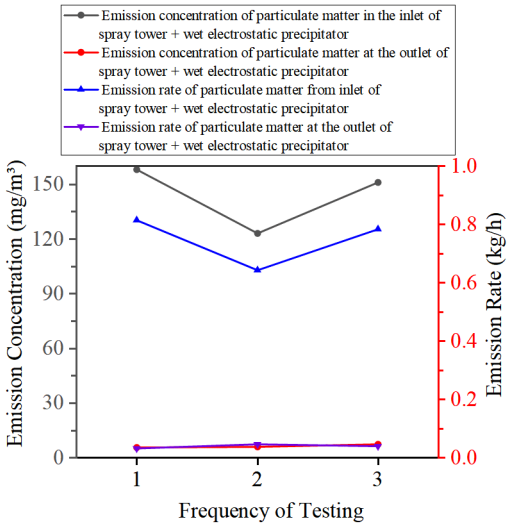

Figure 33. Organized Exhaust Test Results I - Particulate Matter Concentrations Before and After Emission.

© 2025 by the author(s). Distributed under a Creative Commons CC BY license.

Preprints.org (www.preprints.org) | NOT PEER-REVIEWED | Posted: 18 August 2025 doi:10.20944/preprints202508.1164.v1

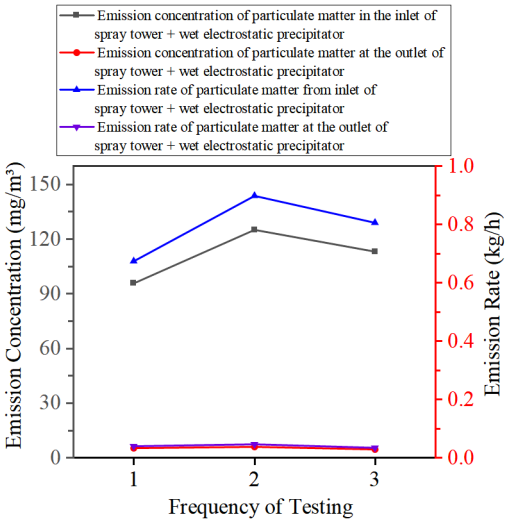

Figure 34. Organized Exhaust Test Results II - Particulate Matter Concentrations Before and After Emission.

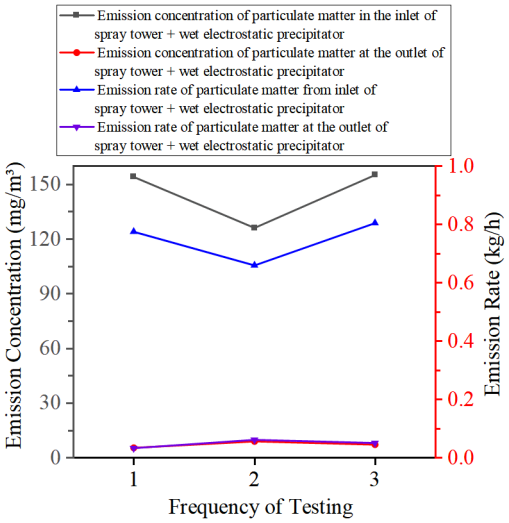

Figure 35. Organized Exhaust Test Results III - Particulate Matter Concentrations Before and After Emissions.

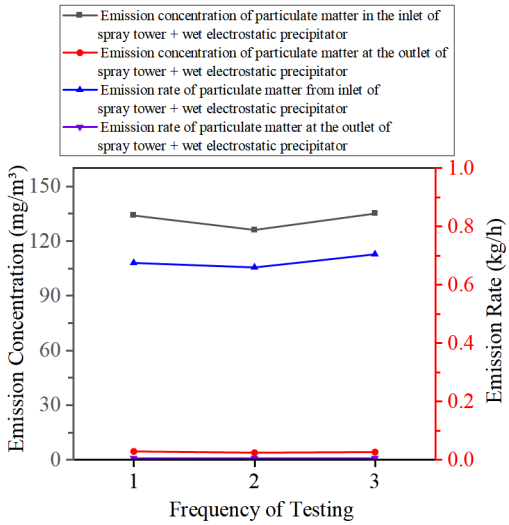

Figure 36. Organized Exhaust Test Results IV - Particulate Matter Concentrations Before and After Emissions.

© 2025 by the author(s). Distributed under a Creative Commons CC BY license.

Preprints.org (www.preprints.org) | NOT PEER-REVIEWED | Posted: 18 August 2025 doi:10.20944/preprints202508.1164.v1

It is known through the results of many field tests:

The inlet concentration of the vertical cellular WESP fluctuates in the range of 95.6-158 mg/m³, and the outlet concentration of particulate matter fluctuates in the range of 3.8-7.4 mg/m³, which is stable and less than 10 mg/Nm³. According to Figure 37, the removal efficiency of particulate matter fluctuates from 95 % to 97 %. From Figure 33, in the second test, the concentration of particulate matter at the inlet of the dust collector is 126 mg/m³, and the concentration at the outlet is only 3.8 mg/m³, which meets the requirement of ultra-low emission, and the removal efficiency is as high as 97 %. The average particulate removal efficiency is 95.88 %, much higher than the design requirement of 80 %, which is better than the traditional dust removal equipment.

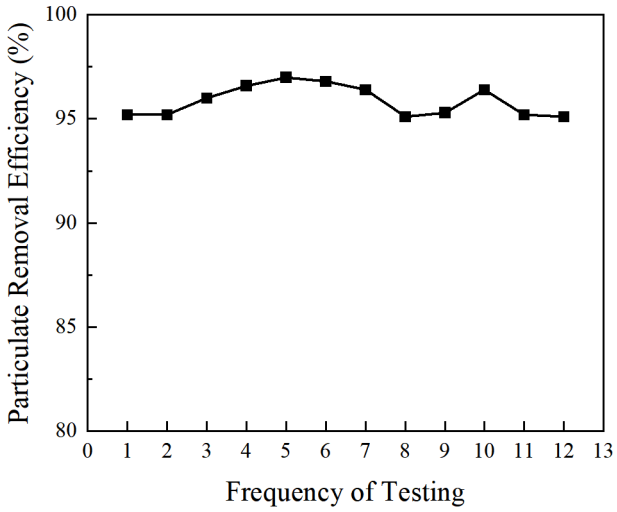

Figure 37. Particulate removal efficiency.

4. Overall Evaluation

(1) Methodological Integration

The study effectively combined CFD simulation with experimental validation to optimize the field of WESP flow. By adjusting the aperture ratio of airflow homogenizing plates (40%–60%), installing deflector plates, and adding a second homogenizing plate, the relative standard deviation of velocity at the anode inlet was reduced from 46% (original model) to 14% (optimized model), meeting the excellent standard ($\sigma_r \leqslant 0.15$). This demonstrates the feasibility of CFD-driven optimization in resolving flow field non-uniformity, a critical challenge in WESP design.

(2) Performance Enhancement

The experimental results showed that the optimized WESP achieved an average dust removal efficiency of 95.88%, significantly higher than the original model (90.67%) and the design requirement (80%). The outlet particle concentration stabilized below 10 mg/Nm³, fulfilling strict emission standards for food and feed processing industries. The improvement in efficiency (5.7% increase) highlights the practical value of the structural modifications, particularly in addressing grease/moisture-induced challenges faced by traditional bag filters.

(3) Limitations and Implications

While this study focuses on vertical honeycomb WESP for medium air capacity (25,000 m³/h), the proposed optimization strategies (e.g., multi-plate homogenization, deflector plates) can be generalized to other WESP configurations or industries with high particulate and aerosol emissions. Future research may explore the impact of water spray parameters and electrode spacing on particles capture efficiency under varying humidity conditions.

(4) Contributions to Environmental Sustainability

© 2025 by the author(s). Distributed under a Creative Commons CC BY license.

Preprints.org (www.preprints.org) | NOT PEER-REVIEWED | Posted: 18 August 2025 doi:10.20944/preprints202508.1164.v1

The optimized vertical honeycomb wet electrostatic precipitator (WESP) achieves an outlet particulate matter concentration ≤ 10 mg/Nm³. Compared with traditional bag filters, it reduces the frequent replacement demand caused by filter bag clogging (approximately 30% annual reduction in filter bag replacement), thereby decreasing industrial solid waste generation. Taking a device with a processing air volume of 25,000 m³/h as an example, it can reduce PM2.5 emissions by about 12.8 tons annually, effectively contributing to regional air pollution prevention and control.

5. Conclusions

(1) Based on the CFD method, the maximum velocity of the anode tube inlet section of the vertical honeycomb WESP is reduced from 2.4 m/s to 1.9 m/s, and the average velocity is reduced from 1.85 m/s to 1.22 m/s by changing the aperture rate and aperture ratio of the airflow homogenizing plate, and increasing the deflector plate and airflow homogenizing plate, which helps to reduce the impact and abrasion of the airflow and improve the overall stability and durability of the dust collector. model by 0.32, reaching an excellent standard, which helps to reduce the impact and wear of the airflow and improve the overall stability and durability of the dust collector.

(2) After many tests, the concentration of particles at the outlet of the vertical cellular WESP is less than 10 mg/Nm³, and the removal efficiency is 95.88%, which is 5.7% higher than that of the original model.

(3) The optimization scheme verified by numerical simulation proved to be feasible through engineering practice, which not only saves the research cost but also provides meaningful guidance for engineering applications.

(4) This study paves the way for integrating CFD-based sustainable design into broader industrial sectors, supporting global transitions toward low-carbon, resource-efficient manufacturing.

6. Patents

This section is not mandatory but may be added if there are patents resulting from the work reported in this manuscript.

Author Contributions: H.G.: methodology (equal); project administration (equal); supervision (equal). Z.Z.: methodology (equal). software (equal); visualization (equal); writing—original draft (equal). L.W.: funding acquisition (equal); resources (equal); methodology (equal); supervision (equal). H.L.: data curation (equal); supervision (equal). X.M.: funding acquisition (equal); resources (equal); supervision (equal). Q.X.: supervision (equal); project administration (equal). Z.L.: resources (equal); project administration (equal). All authors have read and agreed to the published version of the manuscript.

Funding: This research was supported by the "ZHONGYUAN Talent Program" (ZYYCYU202012112), Graduate Education Reform Project of Henan Province(2023SJGLX021Y), the Water Conservancy Equipment and Intelligent Operation and Maintenance Engineering Technology Research Centre in Henan Province (Yukeshi2024-01) and the Scientific and Key Research and Development Program of Henan Province (251111220500)

Data Availability Statement: All data generated or analyzed during this study are included in this published article and its supplementary information files. If there are other data requirements, answers can be obtained from the corresponding author.

Conflicts of Interest: The authors declare no conflicts of interest.

Abbreviations

The following abbreviations are used in this manuscript:

WESP	Wet Electrostatic Precipitator

© 2025 by the author(s). Distributed under a Creative Commons CC BY license.

Preprints.org (www.preprints.org) | NOT PEER-REVIEWED | Posted: 18 August 2025 doi:10.20944/preprints202508.1164.v1

CFD Computational Fluid Dynamics

References

1. Teng, C. Z.; Li, J., Experimental Study on Particle Removal of a Wet Electrostatic Precipitator with Atomization of Charged Water Drops. *Energy Fuels* **2020,** 34, (6), 7257-7268.
2. Yang, F. X.; Liu, H. X.; Feng, P.; Li, Z. H.; Tan, H. Z., Effects of Wet Flue Gas Desulfurization and Wet Electrostatic Precipitator on Particulate Matter and Sulfur Oxide Emission in Coal-Fired Power Plants. *Energy Fuels* **2020,** 34, (12), 16423-16432.
3. Lin, G. Y.; Tsai, C. J.; Chen, S. C.; Chen, T. M.; Li, S. N., An Efficient Single-Stage Wet Electrostatic Precipitator for Fine and Nanosized Particle Control. *Aerosol Sci. Technol.* **2010,** 44, (1), 38-45.
4. Wu, B. B.; Bai, X. X.; Liu, W.; Zhu, C. Y.; Hao, Y.; Lin, S. M.; Liu, S. H.; Luo, L. N.; Liu, X. Y.; Zhao, S.; Hao, J. M.; Tian, H. Z., Variation characteristics of final size-segregated PM emissions from ultralow emission coal-fired power plants in China. *Environ. Pollut.* **2020,** 259, 9.
5. Chen, H. R.; Li, H. T.; Wang, S. T.; Han, Y. Y.; Zhai, X. Y.; Xiao, L. C., Synergistic Humidification and Chemical Agglomeration to Improve Capturing the Fine Particulate Matter by Electrostatic Precipitator. *Coatings* **2024,** 14, (4), 14.
6. Xiao, L. C.; Zhai, X. Y.; Han, Y. Y.; Chen, H. R.; Li, H. T., Experimental Study on Humidification Coagulation and Removal of Fine Particles Using an Electrostatic Precipitator. *Polymers* **2023,** 15, (9), 14.
7. Guo, B. Y.; Hou, Q. F.; Yu, A. B.; Li, L. F.; Guo, J., Numerical modelling of the gas flow through perforated plates. *Chem. Eng. Res. Des.* **2013,** 91, (3), 403-408.
8. Alobaid, F.; Almohammed, N.; Farid, M. M.; May, J.; Rossger, P.; Richter, A.; Epple, B., Progress in CFD Simulations of Fluidized Beds for Chemical and Energy Process Engineering. *Prog. Energy Combust. Sci.* **2022,** 91, 213.
9. Skodras, G.; Kaldis, S.; Sofialidis, D.; Faltsi, O.; Panagiotis, G.; Sakellaropoulos, G. P., Particulate removal via electrostatic precipitators — CFD simulation. *Fuel Processing Technology* **2006,** 87, 623-631.
10. Wang, T.; Wang, P.; Yin, Z. Y.; Laouafa, F.; Hicher, P. Y., Hydro-mechanical analysis of particle migration in fractures with CFD-DEM. *Eng. Geol.* **2024,** 335, 16.
11. Bian, X. M.; Meng, X. B.; Wang, L. M.; MacAlpine, J. M. K.; Guan, Z. C.; Hui, J. F., Negative Corona Inception Voltages in Rod-plane Gaps at Various Air Pressures and Humidities. *IEEE Trns. Dielectr. Electr. Insul.* **2011,** 18, (2), 613-619.
12. Ye, X. L.; Wang, S.; Zhang, H.; An, X. Z.; Guo, B. Y.; Li, L. F., Process simulation and optimization of flow field in wet electrostatic precipitator. *J. Cent. South Univ.* **2020,** 27, (1), 132-143.
13. Liu, X. H.; Gao, Y. L.; Mo, J. H.; Tian, E. Z., Sub-kilovolt electrostatic precipitation for efficient and safe removal of airborne particles. *Sep. Purif. Technol.* **2025,** 361, 10.
14. Tanner, P.; Gorman, J.; Sparrow, E., Flow-pressure drop characteristics of perforated plates. *Int. J. Numer. Methods Heat Fluid Flow* **2019,** 29, (11), 4310-4333.
15. Ning, Z. Y.; Hao, T. H.; Zhang, Z. Y.; Huang, R.; Wang, Z. Y.; Jiang, L. S.; Ning, P., Electrohydrodynamic Flow and Its Impact on Particle Trajectories Inside Wet Electrostatic Precipitator: Experimental and Numerical Analysis. *Environ. Eng. Sci.* **2021,** 38, (6), 513-525.

Disclaimer/Publisher's Note: The statements, opinions and data contained in all publications are solely those of the individual author(s) and contributor(s) and not of MDPI and/or the editor(s). MDPI and/or the editor(s) disclaim responsibility for any injury to people or property resulting from any ideas, methods, instructions or products referred to in the content.

© 2025 by the author(s). Distributed under a Creative Commons CC BY license.